OPEN

Correspondence and
requests for materials
should be addressed to
S.K.S. (sunit@chem.
iitkgp.ernet.in)

Trapping of microwave radiation in hollow polypyrrole microsphere through enhanced internal reflection: A novel approach

Ritwik Panigrahi & Suneel K. Srivastava

Inorganic Materials and Polymer Nanocomposite Laboratory, Department of Chemistry, Indian Institute of Technology, Kharagpur-721302, India.

In present work, spherical core (polystyrene, PS)/shell (polypyrrole, PPy) has been synthesized via in situ chemical oxidative copolymerization of pyrrole (Py) on the surface of sulfonated PS microsphere followed by the formation of hollow polypyrrole (HPPy) shell by dissolving PS inner core in THF. Thereafter, we first time established that such fabricated novel art of morphology acts as a conducting trap in absorbing electromagnetic (EM) wave by internal reflection. Further studies have been extended on the formation of its silver nanocomposites HPPy/Ag to strengthen our contention on this novel approach. Our investigations showed that electromagnetic interference (EMI) shielding efficiency (SE) of HPPy (34.5-6 dB) is significantly higher compared to PPy (20-5 dB) in the frequency range of 0.5-8 GHz due to the trapping of EM wave by internal reflection. We also observed that EMI shielding is further enhanced to 59–23 in 10 wt% Ag loaded HPPy/Ag-10. This is attributed to the simultaneous contribution of internal reflection as well as reflection from outer surface. Such high EMI shielding capacity using conducting polymers are rarely reported.

The modern developments in many electrical and electronic devices, such as mobile phones, computers, TV, radio have become an integral part of day today human life. Simultaneously, development of many other scientific devices and military instruments are also in process[1]. However, proliferation of these devices and wider ongoing instrumentation generates electromagnetic interference (EMI) of radio frequency radiations adversely degrades their performance. This could even completely disrupt functioning of the device performance resulting loss in data storage, energy, time and human health[1,2]. Therefore, it is desirable to isolate these devices/ instruments and prevent from EMI pollution[3]. As a consequence, considerable amount of research has been focused on developing suitable EMI shielding materials either by controlling reflection or absorption[3–9]. For example, TiO_2, SiO_2, ZnO, $BaTiO_3$ and Ni, Co, Fe, $\gamma-Fe_3O_3$, Fe_3O_4 and carbonyl iron has been investigated in EMI shielding due to their high permittivity/permeability[10–14]. However, processing difficulties, chemical repro-ducibility and often inferior mechanical/electrical properties of these materials remained few major hurdles in their development. Additionally, poor dispersion of these materials lead to the seepage of incident radiation through the electromagnetically void space and account for their inferior shielding efficiency[11–17]. Hence, development of an easily processable, light weight, high corrosion resistance material of high permittivity remains an important task in EMI shielding applications. In case of a metal, reflection is one of the key factors in reducing EMI due to its high conductivity and very shallow skin depth[18–20]. However, their processing difficulties, heavy weight, poor flexibility, environmental degradation always became a matter of prime concern[2,21]. On the other hand conducting polymers could carry out reflection and absorption of the EM wave simultaneously leading to provide a significant advantage over the metals[22]. Alternatively, carbon based materials such as carbon black, graphite, carbon nanotube (CNT), carbon nanofibre (CNF), graphene has also been investigated in EMI shielding applications[23–27]. However, carbon black and graphite exhibit poor dispersibility and high percolation threshold leading to low performance in EMI shielding[28–30]. On the contrary, CNT, CNF and graphene could be dispersed in various media[30–34], but their complicated purification and fuctionalization steps including costs make them undesirable for large scale fabrication of EMI shielding materials[3,11,32,33]. For that reason, conducting polymers i.e. polyaniline, polypyrrole and polythiophene etc. has been investigated as suitable alternatives in EMI

shielding application due to their tunable conductivity, corrosion resistance, light weight, easy processability, good environmental stability and tailor-able permittivity[35–38]. Further, conducting polymer nanocomposites has also been widely investigated in last few years. Recently, the conducting polymer nanocomposites derived from core-shell structure has been used in EMI shielding application[39]. Further, it is well known that expulsion of core material in core-shell microsphere could lead fabrication of hollow spherical shell, e.g. SiO_2[40–42], calcium phosphate thin shells[43], mesoporous hydroxyapatite nanoparticles[44], TiO_2[45], metals[46], ZrO_2[47], conducting polymers[48–50]. These hollow sphere are associated with huge interior space, which could be advantageous than the solid materials for many multifaceted applications. In this regard, polypyrrole has received considerable attention due to its high conductivity, light weight, low-cost, large scale processability and environmental stability making it most appropriate material in EMI shielding applications[51–55].

Recently, fabrication of ferromagnetic core/shell polystyrene microsphere (core)/polypyrrole (shell)@nickel has been reported[56]. It acts as effective electromagnetic absorption material due to coating of nickel. Motivated by this, we focused our work on preparation and characterization of polypyrrole hollow microsphere and its silver nanocomposite for EMI shielding application. The formation of such hollow PPy shell could be associated with the lowered particle density. As a consequence, it could lead to reduction in weight of PPy than that prepared through conventional method. Such hollow PPy microsphere could be associated with a novel advantage of reflection as well as absorption of EM wave in EMI shielding applications. It is anticipated that the energy of EM wave passing through the outer PPy shell may not be enough to allow its further penetration through the internal wall of PPy shell. As a result, EM wave could undergo successive internal reflection from the inner wall of PPy shell followed by dissipation of heat energy. Therefore, it would be highly interesting to apply this noble concept in producing enhanced EM wave absorption by applying special art of morphology, never applied on EMI shielding, even till date.

The choice of silver in PPy nanocomposite is guided by its highest conductivity and environmental stability[50]. It is anticipated that presence of Ag in PPy could increase its conductivity resulting in enhanced surface reflection and absorption of EM wave through internal reflections.

Methods

Materials. Potassium persulfate ($K_2S_2O_8$), ammonium persulfate ($(NH_4)_2S_2O_8$, pyrrole and sodium borohydride ($NaBH_4$) were procured from Merck and Sisco Research Laboratory, Mumbai, India respectively. Sodium dodecyl sulfate (SDS) and tetrahydrofuran (THF) were supplied by SRL Pvt., Mumbai, India. Silver nitrate ($AgNO_3$), ethanol, and styrene monomer were purchased from Finar Chemicals Limited, Ahmedabad, Hong Yang Chemical Corporation and Jyoti Lab India respectively.

Preparation sulfonated polystyrene (core) from polystyrene. Monodispersed polystyrene particles (PS) were prepared according to our earlier reported work[50]. In the typical procedure, 140 ml of distilled water was added to 0.1 mmol styrene monomer and magnetically stirred vigorously for about 20 min under nitrogen atmosphere. Subsequently, 10 ml of 0.023 mmol $K_2S_2O_8$ was gradually added to it under stirring condition and kept at 80°C for 24 h. Following this, PS so formed was centrifuged, washed many times with distilled water and subjected to sulfonation by means of concentrated sulfuric acid at 50°C (4 h). Finally, the product (sulfonated polystyrene microsphere) was centrifuged again and washed with distilled water to remove unreacted sulfuric acid, if any.

Preparation of polypyrrole hollow spheres (HPPy). 3 mmol of pyrrole was initially dissolved in dilute hydrochloric acid (50 ml) and subsequently added to PS dispersed in 30 ml distilled under constant stirring at room temperature for 6 h. Subsequently, 1 mmol ammonium persulfate (APS) solution was added to above solution at 0°C and under stirring conditions for 3 h. The grayish black colored product (PS@PPy) so formed was centrifuged, washed with methanol/distilled water mixture to remove oligomers and unreacted monomer followed by its drying at 50°C for 30 h under vacuum. Subsequently, PS core was dissolved by treating PS@PPy with THF at room

temperature. After 2 h, product (hollow PPy microsphere referred as HPPy) was centrifuged, washed with THF/methanol and dried at 50°C for 24 h in vacuum.

Preparation of HPPy/Ag nanocomposites. The fabrication of HPPy/Ag nanocomposites has been carried out using Tollen's reagent following our earlier work[50]. Accordingly, 0.5 mmol SDS and 2 gm HPPy was added to 80 cc of Tollen's reagent (4, 12.7, 25.64 mM with respect to Ag^+) under stirring condition. Subsequently, 15 ml of $NaBH_4$ solution was added drop wise to the earlier prepared solutions (molar ratio $NaBH_4 : AgNO_3 = 1:1$) and kept it at ~80°C for 1 h. The product so formed consisted 2, 5 and 10 wt% Ag were referred as HPPy/Ag-2, HPPy/Ag-5and HPPy/Ag-10 respectively. These were subjected to centrifugation, washed with distilled water, dried in vacuum at 50°C for 48 h.

Characterization. Room temperature x-ray diffraction (XRD) analysis of the samples were performed in the range 5° to 90° on a Phillip, Holland instrument using CuKα radiation (λ=0.1541 nm) and scanning rate of 5° per min. FTIR analysis was carried out with a Perkin-Elmer FTIR Spectrometer RXI using KBr discs in range 400–4000 cm^{-1}.The morphology of the samples were investigated by scanning electron microscopy (SEM) and field emission scanning electron microscopy (FESEM) on JEOL, JSM-5800 scanning microscope and Carl Zeiss operating at 20 kV respectively. TEM images were recorded by TECNAI G^2, SEI (Netherland) operating at 200 kV and Gatan multipole charge-coupled device (CCD) camera. The samples for this purpose were placed as droplet on carbon-coated copper grids and left for drying overnight in vacuum. The gas sorption experiment was carried out using a Quantacrome autosorb iQ automated gas sorption analyzer. 20–25 mg of sample was taken in a 6 mm sample holder without rod. The samples were degassed at 70°C for 2 h prior to the experiment. Ultraviolet-visible (UV-vis) absorption spectrum of samples was recorded on Varian Cary 5000 UV-Visible spectrophotometer. Room temperature dc conductivity of powdered samples compressed in the form of pellets was carried out by four-probe method was using Scientific Equipment Roorkee, Model-LCS-02. S_{11} and S_{12} parameters of samples in compressed pellet form were measured in the frequency range of 100 KHz–20 GHz by ENA series network analyzer, E5071C, Agilent Technology and reflection coefficient (R), transmission coefficient (T) and shielding efficiency (SE) calculated.

Results and discussion

Figure 1 shows the X-ray diffractograms of HPPy, HPPy/Ag-2, HPPy/Ag-5, HPPy/Ag-10 and reduction product of Tollen's reagent. It is noted that a broad peak appeared at around 20–23° in HPPy due to the periodically aligned PPy polymer chains[48,50]. In case of Tollen's reagent reduction product, the presence of intense peaks at 2θ ≈ 38.2°, 44.3°, and 64.5° in XRD correspond to (111), (200) and (220) planes of cubic phase of Ag respectively. [JCPDS file No 00-001-1164]. The diffractograms of HPPy/Ag nanocomposites also showed presence of peaks due to HPPy as well as Ag. Additionally, intensity of these peak increases significantly with increasing Ag loadings.

Figure 2 and supplementary information S1 display FTIR spectra of PS, PS@PPy, HPPy and PPy, HPPy/Ag-2, HPPy/Ag-5 and HPPy/Ag-10 respectively. PS showed presence of strong peaks at ≈ 1491 and 1028 cm^{-1} due to the C=C stretching vibration of the quinoid[57]
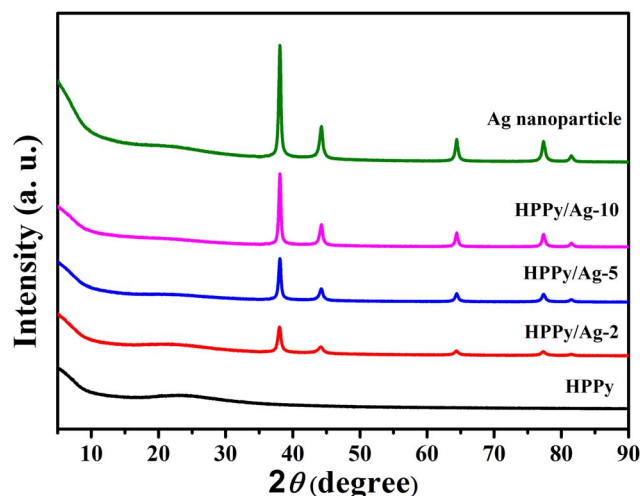

Figure 1 | XRD patterns of HPPy, HPPy/Ag-2, HPPy/Ag-5, HPPy/Ag-10 and Ag nanoparticles.
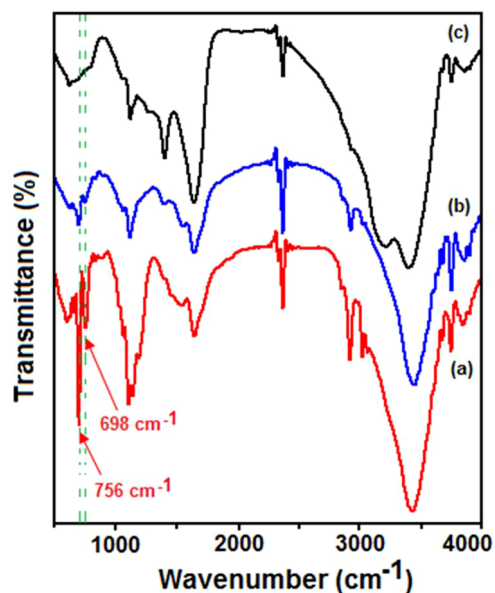
Figure 2 | FTIR spectra of (a) PS, (b) PS@PPy, (c) HPPy.

and benzenoid rings/in-plane bending of C-H bonds[58] of the polymer chain respectively. Further, spectra of PS exhibited many other charactesistic peaks at ≈ 1451 (-C-H bending), 756 (=C-H bending), 698 cm^{-1} (aromatic C-H bending)[59]. Further, peaks appeared in PPy at ≈ 1643/1384, 1233/1117, 1063, 777/680 cm^{-1} corresponds to ring vibration, =C-H in plane vibration, NH_2^+ in plane vibration and C-H out plane vibration respectively[60]. FTIR spectra of PS@PPy showed presence of characteristics peaks corresponding to both PS and PPy. However, intensity of these peaks decreases remarkably in all probability due to the interaction between PS and PPy[61–64]. In addition, appearance of peaks of PS (756, 698 cm^{-1}) and PPy (777, 680 cm^{-1}) confirmed presence of both PS and PPy in PS@PPy. FTIR spectra of PS@PPy, when dessolved in THF, showed disappearance of peaks (756, 698 cm^{-1}) due to PS. However, position and intensity of PPy peaks remain more or less unaltered. These observations strongly suggest that the complete expulsion of PS has taken place from PS@PPy[50].

Figure 3 shows SEM images of as synthesized polystyrene microspheres and PPy coated polystyrene respectively. It clearly indicates the formation of PS microspheres with its diameter in the range of 200–300 nm. When these microspheres are coated with PPy, the surface becomes rough and its overall diameter increases. TEM studies in Figure 4 confirmed the formation of ~50 nm thick PPy coating on the surface of PS microsphere. It is anticipated that the electro-static attraction between the cationic pyrrole and anionic sulphate ions accounts for the adsorption of acidified pyrrole on the surface of sulfonated PS[48].

The morphology investigations of HPPy sample has also been carried out by SEM and TEM in Figure 5 and 6 respectively. The observations based on SEM clearly revealed that PS core disappeared completely leaving aside the microsphere shell of PPy deposited on PS@PPy. Additionally, the presence of fractured surfaces is also evident through SEM images indicating successful expulsion of PS core, a fact also established by TEM. SEM and TEM of HPPy/Ag nanocomposites are also displayed in Figure 6. It is observed that Ag nanoparticles (≈40 nm) are well decorated and appeared as white and black spots on the top of HPPy shell in SEM and TEM respectively. Such enhanced dispersion of Ag over HPPy surfaces could be attributed to the electrostatic attraction between the polycationic HPPy and the anionic SDS modified Ag nanoparticles.

The BET surface area and pore size of PPy and HPPy are summarized in Table 1 (Figure 7). It is observed that HPPy shows much higher surface area as well as pore size compared to PPy. This is probably due to the formation of hollow, porous HPPy shell on expulsion of PS core from PS@PPy as shown SEM and TEM images.

Thermal stability behavior of HPPy and its Ag nanocomposites has been investigated in nitrogen atmosphere and corresponding findings are shown in Figure 8. HPPy exhibits initial weight-loss in TG due to the expulsion of residual water (<139°C). Subsequent and final weight loss in TG observed in the range of ~190–500°C is probably due to degradation of polymer chain[65]. It is also evident that thermo-grams are successively shifted up with increasing silver loading in HPPy with slopped upwards. When 10 wt% is considered in TG, the corresponding temperatures are found to be 119, 229, 250, 283°C for HPPy, HPPy/Ag-2, HPPy/Ag-5 and HPPy/Ag-10 respectively. All these thermal data clearly suggest that thermal stability of the HPPy increases significantly with increasing silver content in HPPy.

Figure 9 shows the typical UV-vis absorption spectra of Ag nanoparticles, HPPy, HPPy/Ag-2, HPPy/Ag-5 and HPPy/Ag-10 respectively. It is noted that absorption band at about 390 nm in SDS stabilized colloidal Ag nanoparticles is due to surface plasmon resonance[66]. A broad band appears at 315 nm in HPPy due to the presence of terpyrrole or quarterpyrrole oligomers[67]. In case of HPPy/Ag nanocomposites, absorption band at 315 nm (PPy) remains intact, though, intensity of absorption band at 390 nm (Ag nanoparticles) appeared very low in intensity due to surface plasmon resonance[68]. It is well known that the surface Plasmon resonance is sensitive to the dielectric properties of the environment[69]. In presence of highly conducting PPy the Ag nanoparticles faces the change in dielectric properties around its surroundings which may reduce the intensity of the absorption band. However
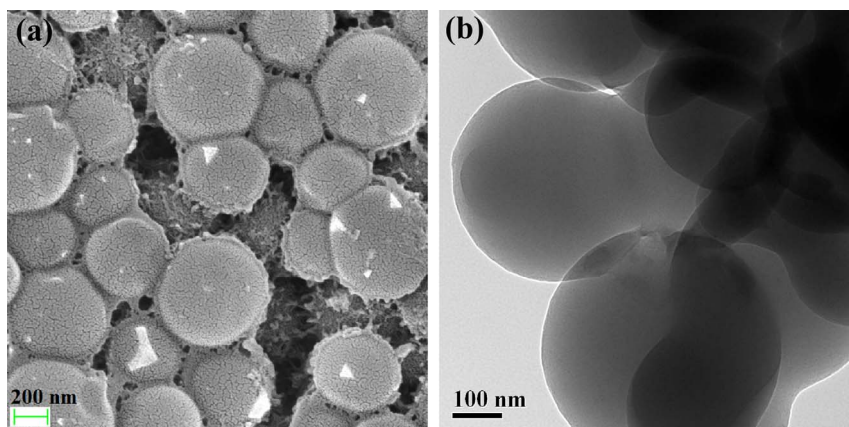

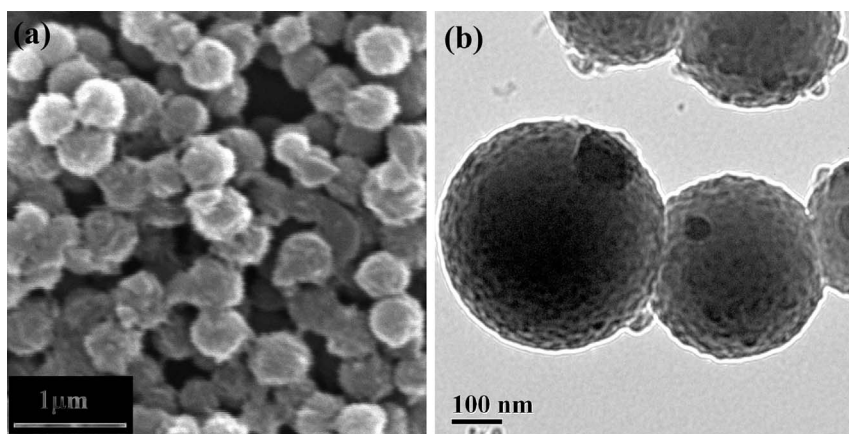Figure 3 | (a) SEM image and (b) TEM image of PS.

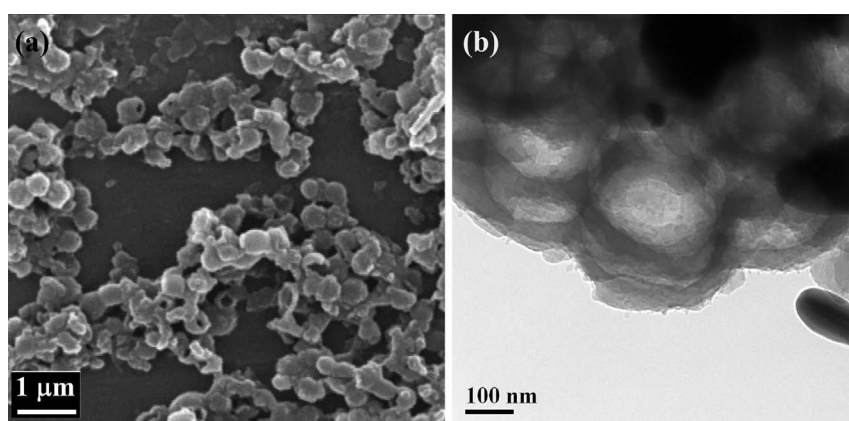Figure 4 | (a) SEM image and (b) TEM image of PS@PPy.

Figure 5 | (a) SEM image and (b) TEM image of HPPy.

UV-vis findings clearly suggest that the Ag nanoparticles form composite with HPPy successfully.

The optical band gap has been calculated from UV absorption spectra using Tauc relation[70]:

$$\alpha h\gamma = A\left(h\gamma - E_g\right)^n \qquad (1)$$

where α, h, γ and E_g, A and n (0.5, 1.5, 2 and 3 according to the mode of transition)[71] are absorption coefficient, Planck's constant, frequency, band gap and constants. In our case, the best fit for the optical absorption data of HPPy and HPPy/Ag is achieved corresponding to n = 0.5 (direct band gap) by plotting $(\alpha h\gamma)^2$ vs. hγ as shown in Figure 9. The extrapolation of the straight portion of the graph on hγ axis at α = 0 gives the band gap for HPPy, HPPy/Ag-2, HPPy/Ag-5 and HPPy/Ag-10 corresponds to their band gap values (E_g) of 4.33, 3.34, 3.25 and 3.02 eV respectively. This finding clearly suggests that optical band gap of PPy decreases with increasing Ag loading possibly due to vis-à-vis increase conductivity[72].

Figure 10 (supplementary information S3) shows the variation of room temperature dc electrical conductivity (σ) as a function of Ag loading in HPPy. These findings clearly indicate that conductivity of HPPy is considerably lower than that of PPy[73]. It may be due to presence of hollow space in each microsphere preventing the formation of solid compressed pellets. Alternatively, the presence of insulating polystyrene, if any, could also deteriorate the conductivity of
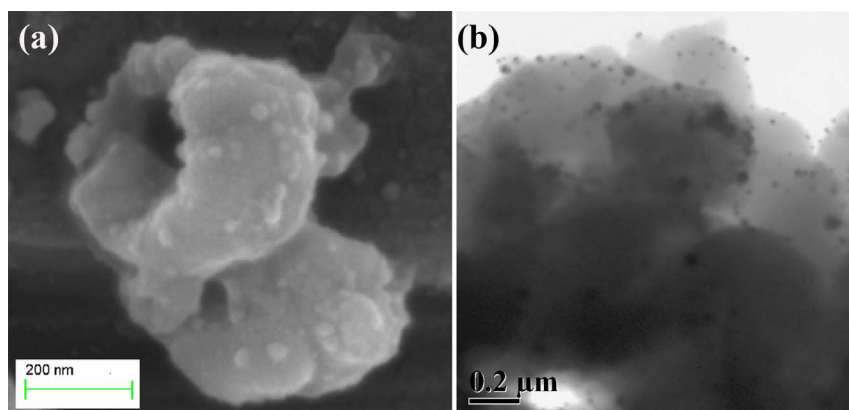

Figure 6 | (a) SEM image and (b) TEM image of HPPy/Ag-10.

Table 1 | Surface area and pore volume of PPy and HPPy

Sample name	Surface area (m²/g)	Pore volume (cc/g)
PPy	1.294	0.01486
HPPy	67.235	0.2684

Figure 8 | TGA of HPPy, HPPy/Ag-2, HPPy/Ag-5, HPPy/Ag-10.

HPPy. Our findings also suggest that conductivity of HPPy with respect to its Ag nanocomposite follows the order HPPy/Ag-10 (2×10^{-2}) ≫HPPy/Ag-5 (5.2×10^{-3})> HPPy/Ag-2 (3.3×10^{-3}) > HPPy (8.2×10^{-4}). The observed increase in conductivity could be attributed to the progressive development of electronic path in HPPy/Ag nanocomposites. The initial small increase in conductivity of HPPy/Ag-2 and HPPy/Ag-5 compared to HPPy could be attributed to the presence of Ag nanoparticles acting as interconnect between the individual HPPy microspheres. Further, abrupt increase in the conductivity in HPPy/Ag-10 could be assigned to the presence of interconnecting network generated by Ag nanoparticles itself[74]. These observations have also been reflected in our subsequent EMI shielding applications.

When electromagnetic radiations are incident on a material, their barrier towards the propagation is due to the contribution from reflection (SE_R), absorption (SE_A) and multiple internal reflections (SE_M). Reflection generally occurs due to the difference in impedance of the corresponding layers (air and interacting material). On the other hand, absorption results in the transfer of electromagnetic energy to be dissipated as heat energy. In contrast, internal multiple reflections involve multiple reflections between the opposite layers (internal) of a material. Accordingly, total shielding efficiency (SE) can be expressed as:

$$SE = SE_R + SE_A + SE_M \qquad (2)$$

When SE values are beyond 12–15 dB, the contribution originating from SE_M could be ignored. As a result, total shielding efficiency, SE (dB) can be expressed as:

$$SE \sim SE_R + SE_A \qquad (3)$$

Mathematically, SE (dB) can be expressed as:

$$SE_T(dB) = 10 \log_{10}(P_T/P_I) \qquad (4)$$

$$= 20 \log_{10}(E_T/E_I) \qquad (5)$$

$$= \log_{10}(H_T/20H_I) \qquad (6)$$

Where, P_I (E_I) and P_T (E_T) are the power (electric field intensity) of incident and transmitted electromagnetic wave respectively.

The reflectance (R) and transmittance (T) of EM wave can be expressed in terms of scattering parameters (S_{11}/S_{22} and S_{12}/S_{21}) as:

$$T = (E_T/E_I)^2 = |S_{12}|^2 = |S_{21}|^2 \qquad (7)$$

$$R = (E_R/E_I)^2 = |S_{11}|^2 = |S_{22}|^2 \qquad (8)$$

From the value of R and T, absorbance (A) can be calculated as[75,76]:
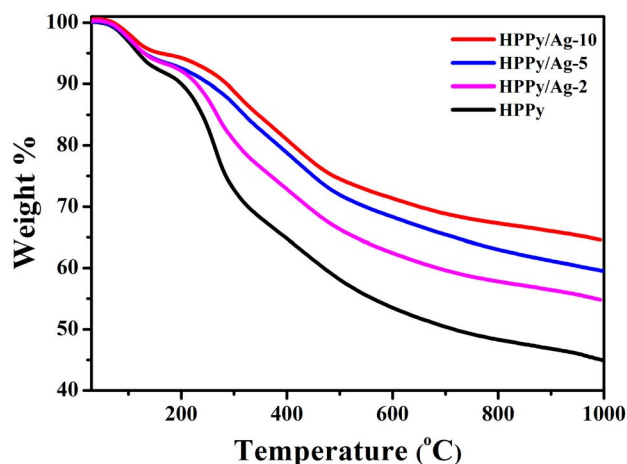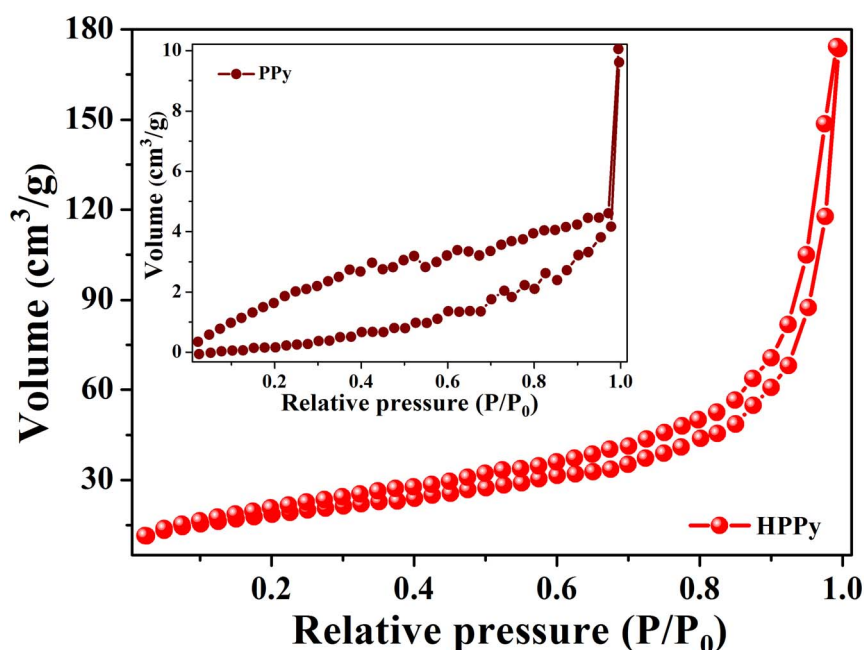
$$A = (1 - R - T) \qquad (9)$$

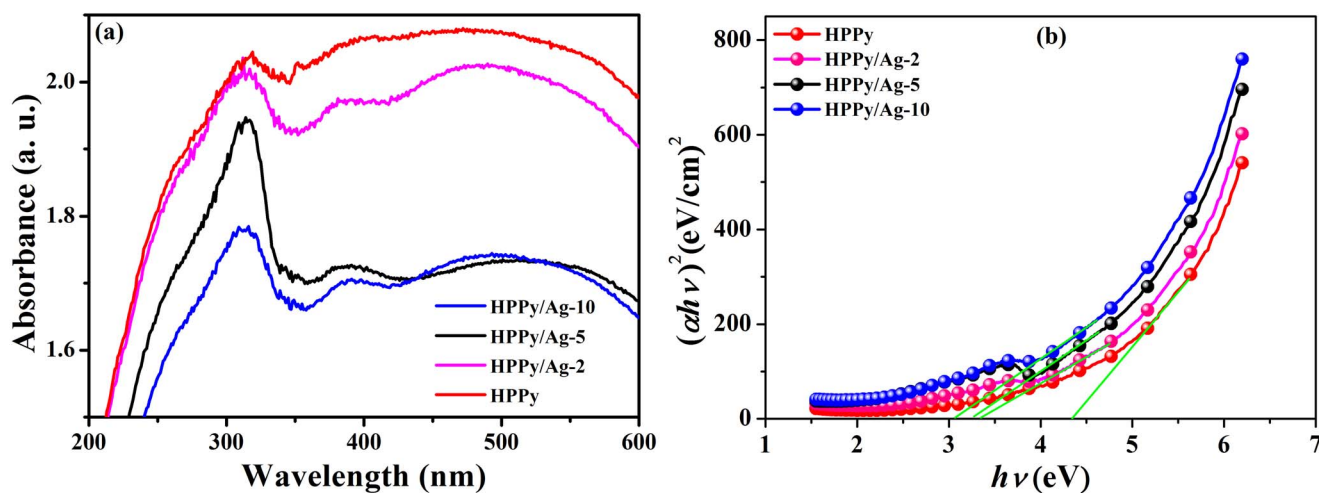Figure 7 | Nitrogen sorption isotherms of HPPy and PPy (inset).

Figure 9 | UV-vis spectra (a) and plot of $(\alpha h\gamma)^2$ vs $h\gamma$ (b) of HPPy, HPPy/Ag-2, HPPy/Ag-5, and HPPy/Ag-10.

Figure 11 shows the variation of reflectance of PPy, HPPy, HPPy/Ag-2, HPPy/Ag-5, HPPy/Ag-10 in frequency range of 0.5–8 GHz. It is inferred that the reflection decreases with increasing incident frequency in all the samples. Figure 11 also shows significant reduction in the reflection value of HPPy ($R_{HPPy} = -0.1$ to -6 dB) compared to PPy ($R_{PPy} = -0.02$ to -2 dB) in HPPy. In all likelihood, the penetration of EM wave through hollow HPPy shell induces random internal reflections. Once these EM radiations are trapped within the shell in this manner, its escaping probability through the outer surface of HPPy could be considerably reduced. We carried this concept for the first time and account for the significant enhancement in EMI shielding of HPPy. R values of HPPy/Ag-2, HPPy/Ag-5 and HPPy/Ag-10 lie in the range of ~-0.25 to -3.5, ~ -0.15 to -2 and ~-0.35 to -3 dB respectively. These findings clearly demonstrate that the reflectance of HPPy/Ag-5 and HPPy/Ag-10 are significantly higher compared to PPy, HPPy or HPPy/Ag-2 probably due to the reflection of EM radiation from the outer surface of the HPPy shell coated with highly conducting Ag nanoparticles[77]. The variation in absorbance values of PPy, HPPy and its Ag nanocomposites in the frequency range 0.5–8 GHz follow the order: HPPy (-16 to -3 dB)~HPPy/Ag-2 (-15 to -3 dB) > HPy/Ag-5 (-23 to -2 dB), > HPPy/Ag-10 (-29 to -4 dB) > PPy (-40 to -10 dB) (Figure 12). These findings clearly show that absorbance is lowest in PPy compared to all other samples. Additionally, HPPy, HPPy/Ag-2 and HPPy/Ag-5, HPPy/Ag-10 together exhibit nearly identical absorbance. However, the superior absorbance of HPPy and HPPy/Ag-2 could be attributed

to internal reflection of the EM wave from the inner shell wall as discussed under reflection earlier. According to our unique art of morphology, the absorbance is anticipated to be independent of Ag loading in HPPy of Ag nanoparticles, which is also established in case of HPPy and HPPy/Ag-2. However, higher Ag loaded HPPy (HPPy/Ag-5 and HPPy/Ag-10) exhibit relatively lower absorbance. This is in all probability due to higher Ag loading on the surface of HPPy, which prohibits the penetration of EM waves in the shell. Interestingly, the absorbance of in HPPy/Ag-2 follows one to one correspondence to HPPy due to the presence of comparably smaller amount of Ag nanoparticles on its surface.

Figure 13 displays the variation of EMI (SE) of PPy, HPPy, HPPy/Ag-2, HPPy/Ag-5, HPPy/Ag-10 samples in the frequency range 0.5–8 GHz. These findings clearly suggest that the corresponding values of EMI (SE) are found to be around ~20 to 5, ~34.5 to 6, ~36.5 to 11.5, ~55.78 to 20, ~59 to 23 dB respectively. Accordingly, HPPy and its Ag loaded nanocomposites exhibit relatively higher EMI (SE) than PPy. It is also noted that EMI (SE) of HPPy/Ag-2 is slightly higher than that of HPPy. On the contrary, EMI (SE) of HPPy/Ag-5 and HPPy/Ag-10 nanocomposites are increased significantly showing one to nearly one correspondence. These findings further reaffirm our earlier view that reflection of EM wave from the inner shell wall of HPPy/Ag-2 is dominating. In contrast, HPPy/Ag-5 and HPPy/Ag-10 undergoes both internal as well as external reflection
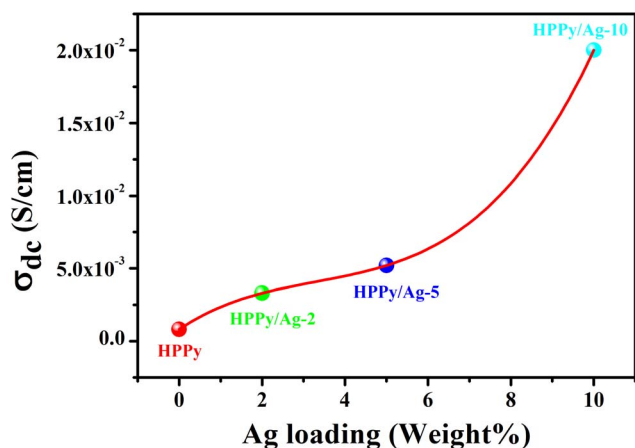

Figure 10 | Variation of room temperature dc conductivity of HPPy and its Ag nanocomposites.
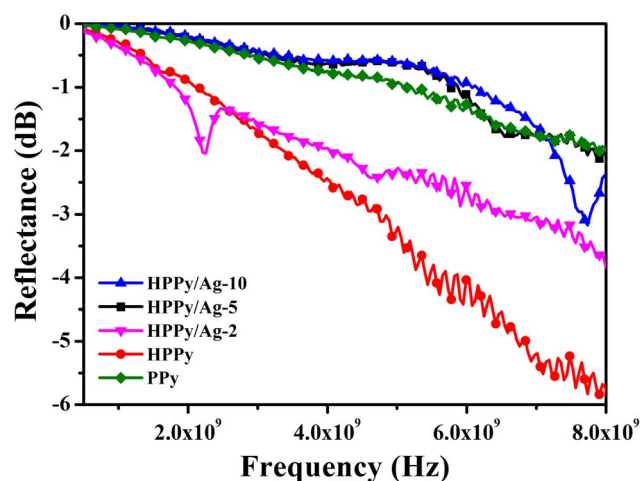

Figure 11 | Variation of reflectance of PPy, HPPy, HPPy/Ag-2, HPPy/Ag-5, HPPy/Ag-10 with varying frequency at 0.5-8 GHz.
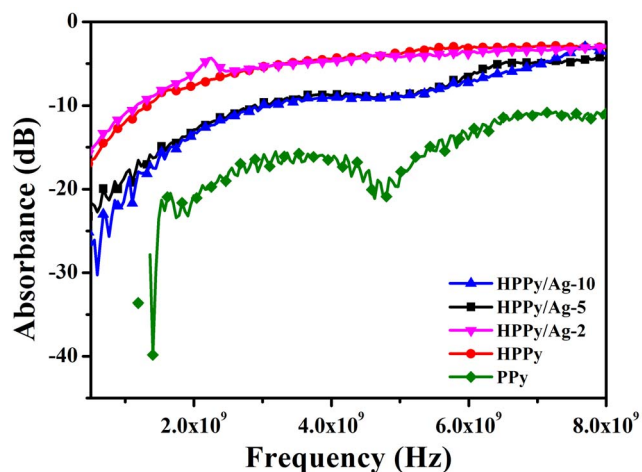
Figure 12 | Variation of absorbance of PPy, HPPy, HPPy/Ag-2, HPPy/Ag-5, HPPy/Ag-10 with varying frequency at 0.5-8 GHz.

simultaneously and accounts for their higher EMI (SE) compared to PPy. This is attributed to the simultaneous contribution of internal reflection as well as reflection from outer surface. Such high EMI shielding capacity using conducting polymers are rarely reported (supplementary information Table 1). The commercial applications require EMI shielding of ~ 20 dB (equal to or less than 1% transmittance of electromagnetic wave). Therefore, it is anticipated this requirement could successfully and most efficiently be fulfilled by HPPy/Ag-5 and HPPy/Ag-10 nanocomposites.

The relative complex permittivity (ε^*) can be expressed as:

$$\varepsilon^* = \varepsilon' - i\varepsilon'' \qquad (10)$$

where ε' and ε'' corresponds to real and imaginary parts respectively. It may be noted that ε' is related to the extent of polarization occurring into the materials representing the ability of electrical energy storage, whereas ε'' symbolizes its dissipation. It may be mentioned that the real part of permittivity is related as:

$$\varepsilon' = C/C_o = Q/Q_o (= Q_o + Q)/Q_o, \qquad (11)$$
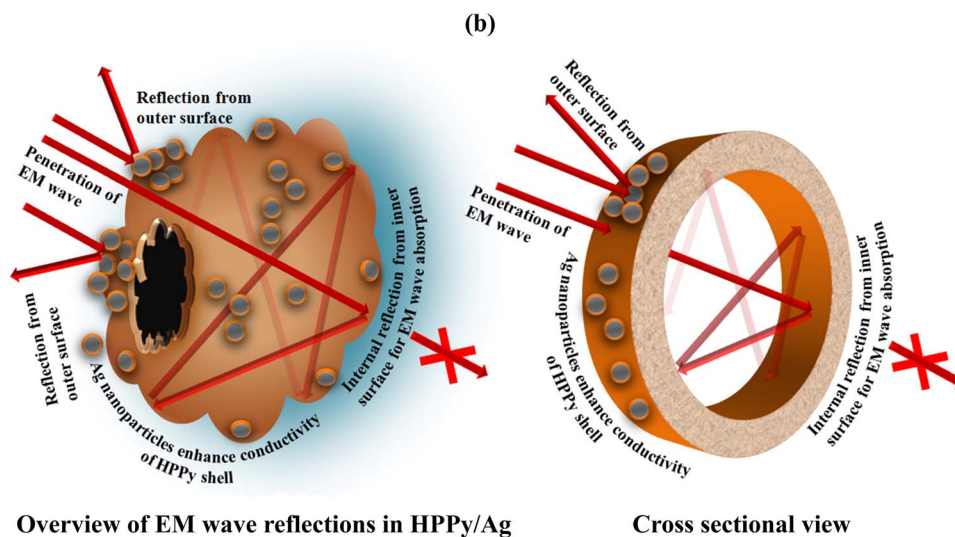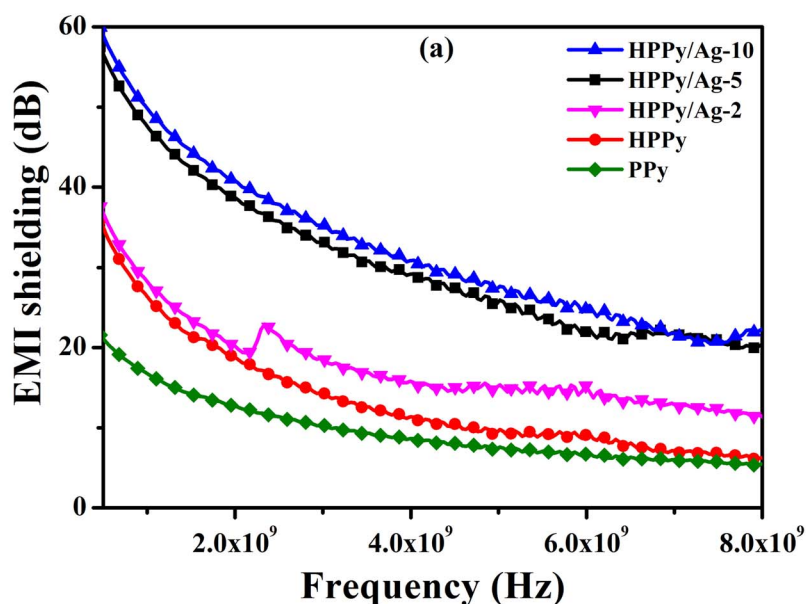

Figure 13 | (a) Variation of EMI shielding of PPy, HPPy, HPPy/Ag-2, HPPy/Ag-5, HPPy/Ag-10 with varying frequency at 0.5-8 GHz, (b) Trapping mechanism of EM wave through enhanced internal reflection in HPPy/Ag: An anticipated scheme.

where Q′, C, Q (and C_o, Q_o) correspond to induced charge, specific capacitance, electric charge of materials under experiment (and in vacuum) respectively. When EM wave interacts with a conducting material, its polarizibility induces dipolar and electrical polarization.

We also investigated the variation of ε′ and ε″ of PPy, HPPy and HPPy/Ag nanocomposites as a function of frequency and calculated these parameters by scattering parameters (S_{11} and S_{21}) directly provided by instrument. Subsequently, standard Nicholson–Ross and Weir theoretical calculations were applied to find out the variation of the ε′ and ε″ with frequency separately (Figure 14)[78–82]. These findings demonstrate that ε′ of HPPy and its silver composites are significantly high compared to PPy in the frequency range of 2–8 GHz. Though, value of ε′ in HPPy (1.5–5) are enhanced nearly 2–2.5 times compared to PPy (0.6–3.2), it is further improved in HPPy/Ag-2 (12–6). In case of HPPy/Ag-5 and HPPy/Ag-10 successive increase of ε′ was also observed with increasing Ag loading but no satisfactory improvements in ε′ is observed in a lower frequency range (0.5–2 GHz). With increasing Ag in HPPy/Ag nanocomposites, conductivity increases leading to enhance polarization. This causes higher electric flux resulting in the increment of permittivity. Similar trend is also observed for ε″ in PPy (0.2–0.75), HPPy (0.7–1.2), HPPy/Ag-2 (5-2), HPPy/Ag-5 (0.9-4.3), HPPy/Ag-10 (0.18-7.8), where the values are found to be relatively much lower compared to ε′ in all the samples over the identical frequency range. In general, the values of both ε′ and ε″ of HPPy are relatively higher compared to PPy, which further increases with increasing Ag loading in HPPy. According to variation of absorbance with frequency discussed in Figure 12, the absorbance (A) is dominant in HPPy and HPPy/Ag-2 enhancing the storage ability of the electrical energy resulting in the enhancement of polarizability. In contrast, when the conductivity of the material is further enhanced by Ag nanoparticles loading, reflection of the EM wave becomes higher than absorbance. As reflection involves dissipation of EM energy, storage capacity through absorption simultaneously decreases. Our studies further strengthen the enhanced trapping of EM wave through internal reflection[83,84]. Further, increased conductivity of HPPy in presence of Ag nanoparticles could account for the enhanced reflection of EM wave from both external as well as internal surface. Further, it may also be noted that the reflection from external surface could affect the neighbouring environment and may not be desirable in a good EMI shielding material. Interestingly, the enhanced successive internal reflection present in HPPy/Ag shell converts EM energy to heat energy leading to the absorption of the EM wave. Our investigations showed that there exists a good balance between these two phenomenons in successfully fabricated HPPy/Ag-2 conducting trap of EM

Figure 15 | Variation of dielectric loss tangent of PPy, HPPy, HPPy/Ag-2, HPPy/Ag-5, HPPy/Ag-10 with varying frequency at 0.5-8 GHz.

wave absorption through enhanced internal reflection (schematically represented in Figure 13.b).

Figure 15 shows dielectric tangent loss factor (tan δ_E) of PPy (0.4–0.2), HPPy (0.5-0.25), HPPy/Ag-2 (0.52-0.34), HPPy/Ag-5 (0.56-0.4), HPPy/Ag-10 (0.57-0.43) in the frequency range 0.5–8 GHz. It is observed that in all cases the tan δ_E value is higher than PPy. Though conductivity of both PPy and HPPy are almost similar, the higher dielectric loss value for HPPy is probably due to absorbance of EM waves due to internal reflection as discussed earlier. In addition it is also observed that with increasing Ag loading, the HPPy/Ag nanocomposites show increasing dielectric loss. The high conductivity of Ag nanoparticles is probably responsible for this observation. Ag has the highest electrical conductivity among other metals so it contains considerable amount of free electrons for movement. As a result collision occurs among each other and causes hindrance in movement. Not only is that, during collision energy of EM wave transferred in to heat to be dissipated. This could probably be responsible for the respective increments in dielectric loss of the materials[82].

Conclusion

Template assisted emulsion polymerization of polystyrene (PS) has been used to prepare hollow polypyrrole (HPPy) and its silver nanocomposites (HPPy/Ag). Such new art of morphology accounts for
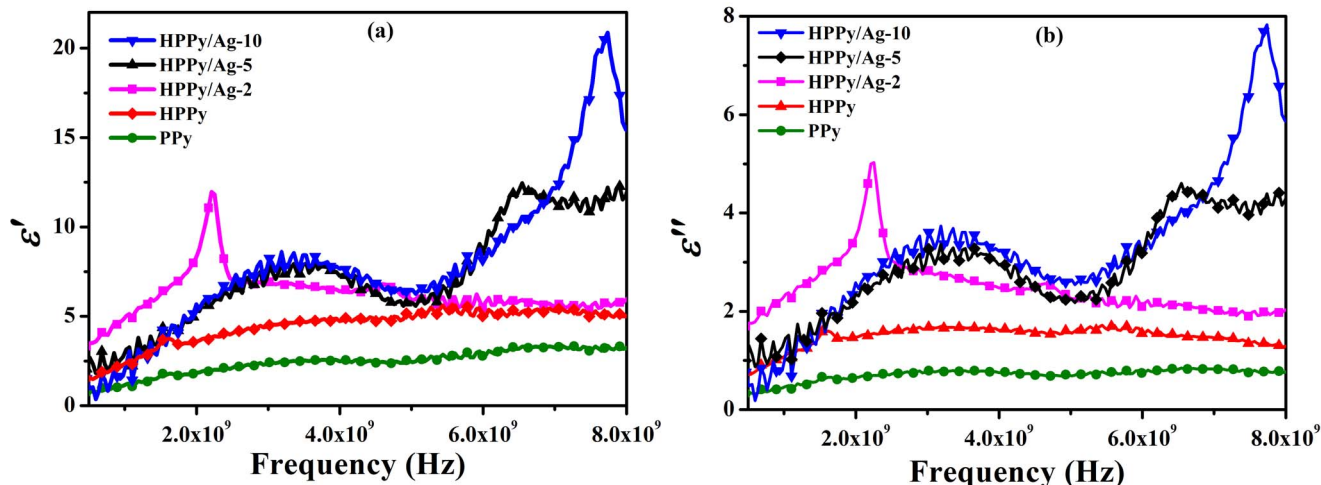

Figure 14 | Variation of (a) real part and (b) imaginary part of complex permittivity of PPy, HPPy, HPPy/Ag-2, HPPy/Ag-5, HPPy/Ag-10 with varying frequency at 0.5-8 GHz.
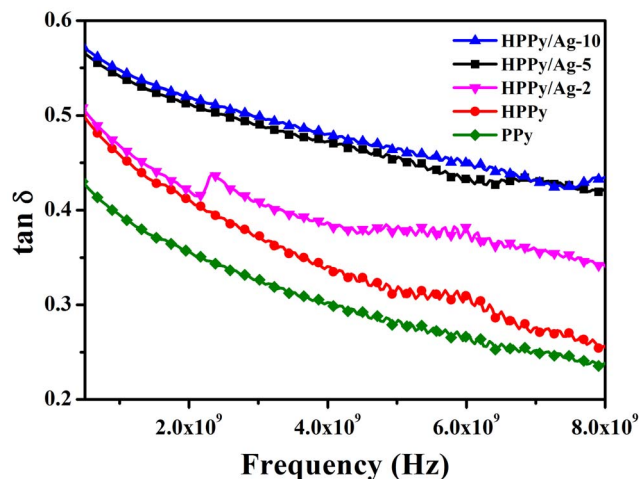
their superior performance in EMI shielding application. It is noted that HPPy exhibited superior performance compared to PPy in EMI shielding. This is attributed to internal reflection of EM wave resulting in enhanced absorbance through our approach of hollow microsphere art of morphology. We also extended our investigations on development of HPPy/Ag nanocomposites. We concluded that HPPy/Ag-2 should show best EMI shielding (36.5-11.5 dB) performance through absorption of EM wave due to preferred internal reflection over reflection from external surface. In contrast, HPPy/Ag-10 exhibited EMI shielding beyond ∼59-23 dB due to high reflection (from outer surface) as well as absorption (through internal reflection) of hollow PPy microsphere. It is anticipated that such hollow microsphere acting as a trap in EMI shielding could also be efficiently extended in many other area of research, such as AM radio, mobile communication, radar etc., where containment of absorption remains a big challenge.

1. Singh, A. P. et al. Encapsulation of g-Fe$_2$O$_3$ decorated reduced graphene oxide in polyaniline core–shell tubes as an exceptional tracker for electromagnetic environmental pollution. *J. Mater. Chem. A* **2**, 3581 (2014).
2. Yang, Y. et al. Novel carbon nanotube−polystyrene foam composites for electromagnetic interference shielding. *Nano Lett.* **5**, 2131 (2005).
3. Ott, H. et al. *Noise reduction techniques in electronic systems.* (Wiley, New York, 1988).
4. Saini, P. et al. Polyaniline–MWCNT nanocomposites for microwave absorption and EMI shielding. *Mater. Chem. Phys.* **113**, 919 (2009).
5. Che, R. C. et al. Microwave absorption enhancement and complex permittivity and permeability of Fe encapsulated within carbon nanotubes. *Adv. Mater.* **16**, 401 (2004).
6. Thomassin, J. M. et al. Multiwalled carbon nanotube/poly(E-caprolactone) nanocomposites with exceptional electromagnetic interference shielding properties. *J. Phys. Chem. C* **111**, 11186 (2007).
7. An, Z. G. et al. Facile preparation and electromagnetic properties of core-shell composite spheres composed of aloe-like nickel flowers assembled on hollow glass spheres. *J. Phys. Chem. C* **113**, 2715 (2009).
8. Xu, P. et al. Synthesis and characterization of novel coralloid Polyaniline/BaFe$_{12}$O$_{19}$ nanocomposites. *J. Phys. Chem. C* **111**, 12603 (2007).
9. Saini, P. et al. Enhanced microwave absorption behaviour of polyaniline-CNT/polystyrene blend in 12.4–18.0 GHz range. *Synth. Met.* **161**, 1522 (2011).
10. Olmedo, L. et al. *Handbook of organic conductive molecules and polymers.* (John Wiley & Sons Ltd. Chichester, 1997).
11. Eswai, A. M. K. et al. Carbon nanotube reinforced composites: Potential and current challenges. *Mater. Des.* **28**, 2394 (2007).
12. Cho, H. S. et al. M-hexaferrites with planar magnetic anisotropy and their application to high-frequency microwave absorbers. *IEEE Trans. Magn.* **35**, 3151 (1999).
13. Haijun, Z. et al. Complex permittivity, permeability, and microwave absorption of Zn- and Ti-substituted barium ferrite by citrate sol/gel process. *Mater. Sci. Eng. B* **96**, 289 (2002).
14. Singh, P. et al. Microwave absorption studies of Ca–NiTi hexaferrite composites in X-band. *Mater. Sci. Eng. B* **78**, 70 (2000).
15. Abbas, S. M. et al. Electromagnetic and microwave absorption properties of (Co^{2+}–Si^{4+}) substituted barium hexaferrites and its polymer composite. *J. Appl. Phys.* **101**, 074105 (2007).
16. Singh, P. et al. Complex permeability and permittivity, and microwave absorption studies of Ca(CoTi)$_x$Fe$_{12}$−2$_x$O$_{19}$ hexaferrite composites in X-band microwave frequencies. *Mater. Sci. Eng. B* **67**, 132 (1999).
17. Shin, J. Y. et al. The microwave absorbing phenomena of ferrite microwave absorbers. *IEEE Trans. Magn.* **29**, 3437 (1993).
18. Joo, J. et al. Electromagnetic interference shielding effiency of polyaniline mixtures and multilayer films. *Synth. Met.* **102**, 1349 (1999).
19. Shui, X. et al. Submicron nickel filaments made by electroplating carbon filaments as a new filler material for electromagnetic interference shielding. *J. Electron. Mater.* **24**, 107 (1995).
20. Li, L. et al. Electrical and mechanical properties of electrically conductive polyethersulfone composites. *Composites* **25**, 215 (1994).
21. Oh, K. W. et al. Adhesion improvement of electroless copper plated layer on PET film. Effect of pretreatment conditions. *Polymer (Korea)* **25**, 302 (2001).
22. Kima, M. S. et al. PET fabric/polypyrrole composite with high electrical conductivity for EMI shielding. *Synth. Met.* **126**, 233 (2002).
23. Kim, H. M. et al. Electrical conductivity and electromagnetic interference shielding of multiwalled carbon nanotube composites containing Fe catalyst. *J. Appl. Phys. Lett.* **84**, 589 (2004).
24. Saini, P. et al. Electrical properties and EMI shielding behavior of highly thermally stable polyaniline/colloidal graphite composites. *Polym. Adv. Technol.* **20**, 355 (2009).
25. Kim, S. H. et al. Electrical properties and EMI shielding characteristics of polypyrrole–nylon 6 composite fabrics. *J. Appl. Polym. Sci.* **87**, 1969 (2003).
26. Zhou, J. et al. Direct incorporation of magnetic constituents within ordered mesoporous carbon-silica nanocomposites for highly efficient electromagnetic wave absorbers. *J. Phys. Chem. C* **114**, 7611 (2010).
27. Yang, Y. et al. Conductive carbon nanofiber-polymer foam structures. *Adv. Mater.* **17**, 1999 (2005).
28. Im, J. S. et al. Fluorination effects of carbon black additives for electrical properties and EMI shielding efficiency by improved dispersion and adhesion. *Carbon* **47**, 2640 (2009).
29. Goyal, R. K. et al. Polyphenylene sulphide/graphite composites for EMI shielding applications. *Adv. Mat. Lett.*, **1**, 143 (2010).
30. Singh, B. P. et al. Designing of multiwalled carbon nanotubes reinforced low density polyethylene nanocomposites for suppression of electromagnetic radiation. *J. Nanopart. Res.* **13**, 7065 (2011).
31. Pandey, S. et al. Improved electromagnetic interference shielding properties of MWCNT–PMMA composites using layered structures. *Nanoscale Res. Lett.* **4**, 327 (2009).
32. Moniruzzaman, M. et al. Polymer nanocomposites containing carbon nanotubes. *Macromolecules* **39**, 5194 (2006).
33. Liang, J. et al. Electromagnetic interference shielding of graphene/epoxy Composites. *Carbon* **47**, 922 (2009).
34. Varrla, E. et al. Functionalized graphene–PVDF foam composites for EMI shielding. *Macromol. Mater. Eng.* **296**, 894 (2011).
35. Saini, P. et al. Electromagnetic interference shielding behavior of polyaniline/graphite composites prepared by in situ emulsion pathway. *J. Appl. Polym. Sci.* **113**, 3146 (2009).
36. Joo, J. et al. Electromagnetic radiation shielding by intrinsically conducting polymers. *J. Appl. Phys. Lett.* **65**, 2278 (1994).
37. Wang, Y. et al. Intrinsically conducting polymers for electromagnetic interference shielding. *Polym. Adv. Technol.* **16**, 344 (2005).
38. Chung, D. D. L. et al. Electromagnetic interference shielding effectiveness of carbon materials. *Carbon* **39**, 279 (2001).
39. Udmale, V. et al. Development trends in conductive nano-composites for radiation shielding. *Orient. J. Chem.* **29**, 927 (2013).
40. Feng, Z. G. et al. A facile route to hollow nanospheres of mesoporous silica with tunable size. *Chem. Commun.* **23**, 2629 (2008).
41. Wang, T. et al. Uniform hollow mesoporous silica nanocages for drug delivery in vitro and in vivo for liver cancer therapy. *J. Mater. Chem.* **21**, 5299 (2011).
42. Wang, T. et al. Multifunctional hollow mesoporous silica nanocages for cancer cell detection and the combined chemotherapy and photodynamic therapy. *ACS Appl. Mater. Interfaces* **3**, 2479 (2011).
43. Bastakoti, B. P. et al. Inorganic–organic hybrid nanoparticles with biocompatible calcium phosphate thin shells for fluorescence enhancement. *Chem. Asian J.* **8**, 1301 (2013).
44. Yang, Y. H. et al. Hollow mesoporous hydroxyapatite nanoparticles (hmHANPs) with enhanced drug loading and pH-responsive release properties for intracellular drug delivery. *J. Mater. Chem. B* **1**, 2447 (2013).
45. Yang, J. et al. Synthesis of hollow silica and titania nanospheres. *Chem. Mater.* **20**, 2875 (2008).
46. Esfahani, H. et al. A. Rational synthesis of Pt spheres with hollow interior and nanosponge shell using silica particles as template. *Chem. Commun.* **47**, 3885 (2011).
47. Tang, S. et al. Hollow mesoporous zirconia nanocapsules for drug delivery. *Adv. Funct. Mater.* **20**, 2442 (2010).
48. Feng, X. et al. Polyaniline/Au composite hollow spheres: synthesis, characterization, and application to the detection of dopamine. *Langmuir* **22**, 4384 (2006).
49. Zha, Z. et al. Polypyrrole hollow microspheres as echogenic photothermal agent for ultrasound imaging guided tumor ablation. *Sci. Rep.* **3**, 2360 (2013).
50. Panigrahi, R. et al. Ultrasound assisted synthesis of a polyaniline hollow microsphere/Ag core/shell structure for sensing and catalytic applications. *RSC Adv.* **3**, 7808 (2013).
51. Lim, S. P. et al. In-situ electrochemically deposited polypyrrole nanoparticles incorporated reduced graphene oxide as an efficient counter electrode for platinum-free dye-sensitized solar cells. *Sci. Rep.* **4**, 5305 (2014).
52. Wu, J. et al. High-performance polypyrrole nanoparticles counter electrode for dye-sensitized solar cells. *J. Power Sources* **181**, 172 (2008).
53. Gangopadhyay, R. et al. Conducting polymer nanocomposite: a brief overview. *Chem. Mater.* **12**, 608 (2000).
54. Mermilliod, N. et al. A study of chemically synesized polypyrrole as electrode material for battery applications. *J. Electrochem. Soc.* **133**, 1073 (1986).
55. Kuhn, H. H. et al. Toward real applications of conductive polymers. *Synth. Met.* **71**, 2139 (1995).
56. Li, W. et al. Preparation and electromagnetic properties of core/shell polystyrene@polypyrrole@nickel composite microspheres. *ACS Appl. Mater. Interfaces* **5**, 883 (2013).
57. Huang, K. et al. Self-assembled polyaniline nanostructures with photo isomerization function. *Chem. Mater.* **14**, 3486 (2002).
58. Li, G. et al. Synthesis of dendritic polyaniline nanofibers in a surfactant Gel. *Macromolecules* **37**, 2683 (2004).

59. Sertchook, H. *et al.* Submicron silica/polystyrene composite particles prepared by a one-step Sol-Gel Process. *Chem. Mater.* **15**, 1690 (2003).

60. Dallas, P. *et al.* Interfacial polymerization of pyrrole and in situ synthesis of polypyrrole/silver nanocomposites. *Polymer* **48**, 2007 (2007).

61. Jing, S. *et al.* Synthesis and characterization of Ag/polypyrrole nanocomposites based on silver nanoparticles colloid. *Mater. Lett.* **61**, 4528 (2007).

62. Wei, Y. *et al.* One-step UV-induced synthesis of polypyrrole/Ag nanocomposites at the water/ionic liquid interface. *Nanoscale Res. Lett.* **5**, 433 (2010).

63. Xing, S. *et al.* One-step synthesis of polypyrrole–Ag nanofiber composites in dilute mixed CTAB/SDS aqueous solution. *Mater. Lett.* **61**, 2040 (2007).

64. Dias, H. V. R. *et al.* Greener method for high quality polypyrrole. *Polymer* **47**, 7349 (2006).

65. Wei, Y. *et al.* Thermal analysis of chemically synthesized polyaniline and effects of thermal aging on conductivity. *J. Polym. Sci. Part A: Polym. Chem.* **27**, 4351 (1989).

66. Mirkin, C. A. *et al.* Programming the assembly of two- and three-dimensional architectures with DNA and nanoscale inorganic building blocks. *Inorg. Chem.* **39**, 2258 (2000).

67. Zotti, G. *et al.* Well-defined pyrrole oligomers: Electrochemical and UV/vis studies. *Adv. Mater.* **4**, 798 (1992).

68. Selvan, S. T. *et al.* Block copolymer mediated synthesis of gold quantum dots and novel gold-polypyrrole nanocomposites. *J. Phys. Chem. B* **103**, 7441 (1999).

69. Xia, H. S. *et al.* Ultrasonic irradiation: A novel approach to prepare conductive polyaniline/nanocrystalline titanium oxide composites. *Chem. Mater.* **14**, 2158 (2002).

70. Tauc, J. *et al.* Optical properties and electronic structure of amorphous Ge and Si. *Mater. Res. Bull.* **3**, 37 (1968).

71. Subramanian, S. *et al.* Effect of structural, electrical and optical properties of electrodeposited bismuth selenide thin films in polyaniline aqueous medium. *Mater. Chem. Phys.* **107**, 392 (2008).

72. Benramache, S. *et al.* Correlation between electrical conductivity–optical band gap energy and precursor molarities ultrasonic spray deposition of ZnO thin films. *J. Semicond.* **34**, 113001 1-5 (2013).

73. Puanglek, N. *et al.* Enhancement of electrical conductivity of polypyrrole and its derivative. *Sci. J. UBU* **1**, 35 (2010).

74. Attia, M. F. *et al.* One-step UV-induced modification of cellulose fabrics by polypyrrole/silver nanocomposite films. *J. Colloid Interf. Sci.* **393**, 130 (2013).

75. Li, N. *et al.* Electromagnetic interference (EMI) shielding of single-walled carbon nanotube epoxy composites. *Nano Lett.* **6**, 1141 (2006).

76. Wang, J. *et al.* Ordered mesoporous carbon/fused silica composites. *Adv. Funct. Mater.* **18**, 2995 (2008).

77. Gelves, G. A. *et al.* Highly electrically conductive and high performance EMI shielding nanowire/polymer nanocomposites by miscible mixing and precipitation. *J. Mater. Chem.* **21**, 829 (2011).

78. Nicolson, A. M. *et al.* Measurement of the intrinsic properties of materials by time-domain techniques. *IEEE Trans. Instrum. Meas.* **IM-19**, 377 (1970).

79. Ling, J. *et al.* Facile preparation of lightweight microcellular polyetherimide/ graphene composite foams for electromagnetic interference shielding. *ACS Appl. Mater. Interfaces* **5**, 2677 (2013).

80. Nicolson, A. M. *et al.* Broad-band microwave transmission characteristics from a single measurement of the transient response. *IEEE Trans. Instrum. Meas.* **IM-17**, 395 (1968).

81. Wang, C. *et al.* The electromagnetic property of chemically reduced graphene oxide and its application as microwave absorbing material. *Appl. Phys. Lett.* **98**, 072906 (2011).

82. Chen, Y. *et al.* Electromagnetic interference shielding efficiency of polyaniline composites filled with graphene decorated with metallic nanoparticles. *Compos. Sci. Technol.* **80**, 80 (2013).

83. Saini, P. *et al.* Improved electromagnetic interference shielding response of poly (aniline)-coated fabrics containing dielectric and magnetic nanoparticles. *J. Phys. Chem. C* **116**, 13403 (2012).

84. Panigrahi, R. *et al.* Selective reduction of graphite oxide: A novel approach. *RSC Adv.* **4**, 53055 (2014).

Acknowledgments

Author contributions

The proposed work has been done by R.P. under supervision of S.K.S. and equal contribution has been made in writing and review of this manuscript.

Additional information

Supplementary information accompanies this paper at http://www.nature.com/ scientificreports

Competing financial interests: The authors declare no competing financial interests.

How to cite this article: Panigrahi, R. & Srivastava, S.K. Trapping of microwave radiation in hollow polypyrrole microsphere through enhanced internal reflection: A novel approach. *Sci. Rep.* **5**, 7638; DOI:10.1038/srep07638 (2015).